J. Fluid Mech. (1973), *vol.* 61, *part* 2, *pp.* 401–413
Printed in Great Britain

Hysteresis and nonlinear detuning in a spatial-resonance phenomenon

By IAN HUNTLEY† AND RONALD SMITH
Fluid Mechanics Research Institute, University of Essex

(Received 21 February 1973 and in revised form 16 July 1973)

The experimental work of Franklin, Price & Williams (1973) shows that for moderately large driving amplitudes there are features of spatial resonance that are not predicted by the model representation of Mahony & Smith (1972). We here derive an alternative model, which remains valid for moderately large driving amplitudes, and we are able to obtain a theoretical description of both hysteresis and nonlinear detuning of the low frequency wave response. An experiment in which surface waves were generated by a sinusoidal pressure field at the free surface (and which corresponds almost exactly to the theoretical problem) was conducted in order to test these predictions.

1. Introduction

Spatial resonance is a term which describes a strong interaction between two classes of waves, these having related modal shapes but quite disparate frequencies. In their recent theoretical paper, Mahony & Smith (1972) put forward a model explaining the onset of low frequency waves in a system when high frequency waves are driven at a frequency close to resonance. The neutral-stability curve for this phenomenon (that is, the relationship between the driving force and frequency required to excite waves with zero growth rate) was experimentally checked by Huntley (1972) and Franklin, Price & Williams (1973); in both experimental configurations the agreement between theory and experiment was quite good. The latter experiments, however, brought to light two interesting features which occur at moderately large driving amplitudes.

First, the theory predicts a neutral-stability curve with an asymptote at the resonance frequency whereas the experiments of Franklin, Price & Williams give a neutral-stability curve which remains finite at the resonance frequency. These are sketched in figure 1. Second, for constant drive and slowly varying frequency the steady-state amplitude of the low frequency wave exhibits hysteresis; this is illustrated in figure 2.

In the appendix to their paper, Mahony & Smith give an intricate argument showing that the presence of harmonics of the forced high frequency wave could explain the frequency shift of the neutral-stability curve. In this paper we implicitly represent such harmonics by allowing the high frequency response to have soft-spring behaviour, and we obtain the result that the neutral-stability curve asymptotes to the nonlinear resonance frequency.

† Present address: Engineering Department, University of Leicester.

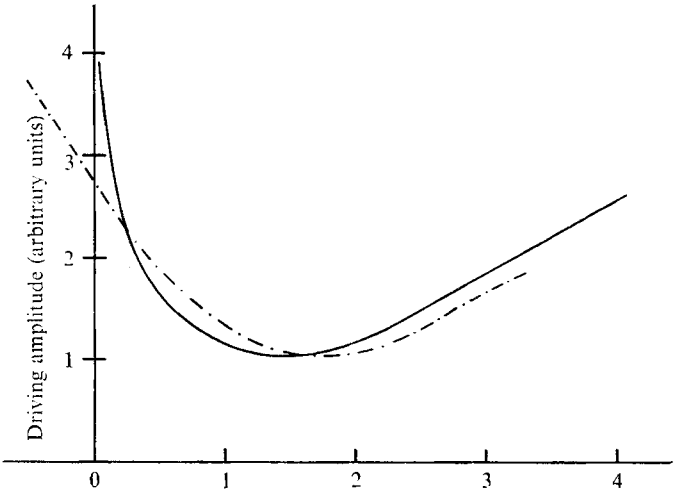

FIGURE 1. Curves showing the threshold of stability. ——, theory; –·–·–, experiment.

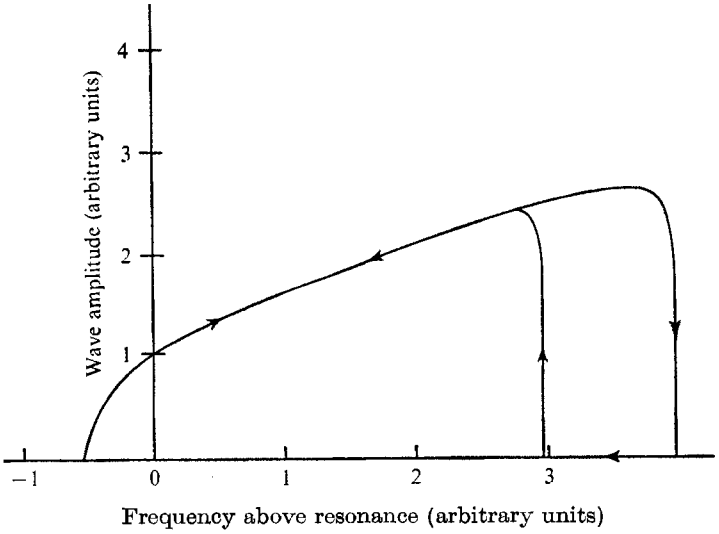

FIGURE 2. Experimental curve showing the low frequency wave amplitude.

According to the present theory the energy fed into the low frequency waves depends on the intensity of the high frequency waves in a frequency band about resonance. The presence of a strong low frequency wave induces a frequency splitting of the high frequency waves, and if several of these frequencies were in the relevant band then the energy fed into the low frequency waves would differ markedly from the energy fed in the absence of strong low frequency waves. Hence it is conceivable that viscous damping would preclude the onset of small amplitude, low frequency waves, yet if strong waves were already established they could persist. Mahony & Smith include three high frequency waves but do

not predict hysteresis; here we permit an arbitrary amount of frequency splitting and hysteresis is predicted.

In order to test quantitatively the theoretical predictions it would be necessary either to carry out theoretical calculations for the shallow-water experiment of Franklin, Price & Williams or else to perform an experiment on the deep-water situation studied by Mahony & Smith. Here we choose the latter, and the results of these experiments together with a comparison with the theoretical predictions are given in § 6.

2. Model equations

Schematically we combine the equations of motion and boundary conditions for a weakly damped, forced, nonlinear system into a single equation for (say) the velocity potential $u(\mathbf{x}, t)$:

$$\langle v, u_{tt} + Lu \rangle = \langle v, (Mu)_t + Nu + 4\Omega B \cos \omega t \rangle. \tag{1}$$

Here $\langle\ \rangle$ denotes the inner product (which would usually be the L_2 integral inner product) for some Hilbert space in which L is a linear self-adjoint operator, v is an arbitrary element in the domain of L, M is a linear operator representing dissipation, N represents the weak nonlinearities and $4\Omega B$ is the driving amplitude.

In the theory of Mahony & Smith, the velocity potential of the wave motion is represented by

$$u = \{(\Phi_0 e^{i\omega t} + \Phi_+ e^{i(\omega+\sigma)t} + \Phi_- e^{i(\omega-\sigma)t}) X(\mathbf{x}) + \eta e^{i\sigma t} Y(\mathbf{x}) + *\}, \tag{2}$$

where ω and σ denote the high and low frequencies, $*$ denotes the complex conjugate of each term inside the bracket, η, Φ_0, Φ_+ and Φ_- are slowly varying functions of time, and the modal shapes $X(\mathbf{x})$ and $Y(\mathbf{x})$ are normalized solutions of the linear eigenvalue problems

$$\langle v, -\Omega^2 X + LX \rangle = 0,$$
$$\langle v, -\sigma^2 Y + LY \rangle = 0$$

(that is, they are free modes of the undamped linear system).

As a consequence of (2), the dissipation term in (1) can be represented (in an integral, not a pointwise sense) by

$$-Mu = \{2\nu(\Phi_0 e^{i\omega t} + \Phi_+ e^{i(\omega+\sigma)t} + \Phi_- e^{i(\omega-\sigma)t}) X(\mathbf{x}) + 2\nu' \eta e^{i\sigma t} Y(\mathbf{x}) + \chi_1 + *\}, \tag{3}$$

where χ_i will be used to represent terms whose time or space structure is such that they play no role in the interactions. If we retain only quadratic nonlinearities, we can represent the nonlinear term in (1) by

$$-Nu = \{2\sigma\beta(\Phi_0 \Phi_-^* + \Phi_0^* \Phi_+) Y e^{i\sigma t} + 2\Omega\alpha(\Phi_- \eta e^{i\omega t} + \Phi_0 \eta e^{i(\omega+\sigma)t}) X$$
$$+ 2\Omega\alpha^*(\Phi_+ \eta^* e^{i\omega t} + \Phi_0 \eta^* e^{i(\omega-\sigma)t}) X + \chi_2 + *\}, \tag{4}$$

where we have already used the Mahony & Smith assumptions about the modal shapes, replacing X^2 and XY by Y and X respectively. Here ν and ν' are real

constants and α and β are complex constants all dependent on the modal shapes X and Y. For the problems studied by Mahony & Smith, Huntley and Franklin, Price & Williams the coupling constants α and β are real and positive; to simplify the subsequent analysis we therefore assume that this is so.

We are now in a position to recover trivially Mahony & Smith's equations. Setting $v \equiv Y$ in (1) and restricting attention to terms with time dependence $e^{i\sigma t}$ gives us

$$\eta_t + \nu'\eta = i\beta(\Phi_0 \Phi_-^* + \Phi_0^* \Phi_+) + (i/\sigma)(\tfrac{1}{2}\eta_{tt} - \nu'\eta_t).$$

Since η is a slowly varying function of time we neglect the final two terms in this equation to obtain equation (14*d*) of Mahony & Smith. Likewise, setting $v \equiv X$ and restricting attention to terms with time dependence $e^{i\omega t}$, $e^{i(\omega+\sigma)t}$ and $e^{i(\omega-\sigma)t}$ gives us equations (14*a*), (14*b*) and (14*c*) of Mahony & Smith, the only assumption being that both σ and $|\omega - \Omega|$ are small compared with Ω.

In the above theory it is implicit that the side-band frequencies $\omega \pm \sigma$ are not strongly excited, since otherwise the ignored nonlinear terms $\eta\Phi_+$ and $\eta^*\Phi_-$ would drive significant amounts of the side bands $\omega \pm 2\sigma$, which in turn would drive other side bands. Thus it is natural to attribute features such as hysteresis, which occur for moderately high driving amplitudes, to this cascade of side-band frequencies.

A generalization of the representations (2), (3) and (4) that can represent a side-band cascade is

$$u = f(t)\, X(\mathbf{x}) + g(t)\, Y(\mathbf{x}), \tag{5}$$

$$-Mu = 2\nu f X + 2\nu' g Y + \chi_3, \tag{6}$$

$$-Nu = \sigma\beta(f^2)\, Y + 2\Omega\alpha(fg)\, X + 2\lambda(f^3)\, X + 2\kappa(g^3)\, Y + \chi_4. \tag{7}$$

It is feasible that, although the interactions between the two classes of waves are weak, the individual waves are sufficiently nonlinear that there are strong self-interactions. For the particular experiments being modelled here the resonant bandwidths are so narrow that despite the small amplitudes of the waves the self-interactions lead to nonlinear resonance frequency shifts that are comparable with the resonant bandwidths. Thus in (7) we have included those cubic terms with the correct modal shape, which thus correspond to the self-interactions.

Using (1) we can now derive the following coupled ordinary differential equations:

$$f_{tt} + \Omega^2 f + 2\nu f_t + 2\Omega\alpha fg + 2\lambda f^3 = 4\Omega\langle X, B\rangle \cos\omega t, \tag{8}$$

$$g_{tt} + \sigma^2 g + 2\nu' g_t + \sigma\beta f^2 + 2\kappa g^3 = 0, \tag{9}$$

which we study further in §3.

3. Multiple time scales

In order to do a systematic analysis of the model equations (8) and (9) we must specify the relative sizes of the frequencies Ω, σ, ν, ν', $\lambda f^2/\Omega$ and $\kappa g^2/\sigma$. The corresponding sizes for $|\omega - \Omega|$, f, g and B then follow from the fact that we are concerned with such features as the neutral-stability curve. To describe the known examples of spatial resonance it suffices to introduce two *independent*

Authors	$\tilde{\sigma}$	$\tilde{\nu}'$
Huntley (1972)	0·02	0·001
Franklin, Price & Williams (1973)	0·004	0·003
Huntley & Smith (1973)	0·005	0·004

TABLE 1

small parameters $\tilde{\sigma} = \sigma/\Omega$ and $\tilde{\nu}' = \nu'/\sigma$ (see table 1), and to scale the other terms via

$$\Delta \equiv (\omega - \Omega)/\sigma, \quad \tilde{\nu} = \nu/\sigma, \quad \tilde{\lambda} = \lambda\nu'/\Omega, \quad \tilde{\kappa} = \kappa\sigma/\nu',$$
$$\tilde{f} = f(\sigma\nu')^{-\frac{1}{2}}, \quad \tilde{g} = g/\sigma, \quad \tilde{B} = \langle X, B\rangle \sigma^{-\frac{3}{2}}\nu'^{-\frac{1}{2}}.$$

Equations (8) and (9) then become

$$\Omega^{-2}\tilde{f}_{tt} + \tilde{f} + 2\tilde{\sigma}\{\tilde{\nu}\Omega^{-1}\tilde{f}_t + \alpha\tilde{f}\tilde{g} + \tilde{\lambda}\tilde{f}^3\} = 4\tilde{\sigma}\tilde{B}\cos(\Omega t + \sigma\Delta t), \tag{10}$$

$$\sigma^{-2}\tilde{g}_{tt} + \tilde{g} + 2\tilde{\nu}'\{\sigma^{-1}\tilde{g}_t + \tfrac{1}{2}\beta\tilde{f}^2 + \tilde{\kappa}\tilde{g}^3\} = 0. \tag{11}$$

For simplicity, we shall restrict our attention to these particular equations but we recall that several assumptions were used in deriving the model equations (8) and (9), and although these assumptions are justified for the known examples of spatial resonance, it is possible to envisage circumstances in which other scalings would be required.

We shall use a multiple time scales approach to solve (10) and (11) (Cole 1968, chap. 3), and so we put

$$\tilde{t} = \Omega t, \quad \tau = \sigma t, \quad T = \nu' t.$$

Physically, $\tilde{t}$ then corresponds to the time scale of the forced high frequency oscillations, τ to that of the free low frequency oscillations and T to the evolution scale of any instabilities (that is, the time taken to reach a steady state). We now formally put

$$\Omega^{-1}\frac{d}{dt} = \frac{\partial}{\partial\tilde{t}} + \tilde{\sigma}\frac{\partial}{\partial\tau} + \tilde{\nu}'\tilde{\sigma}\frac{\partial}{\partial T},$$

and regard $\tilde{f}$ and $\tilde{g}$ as functions of the three independent variables $\tilde{t}$, τ and T.

We put

$$f = f_{00} + \sigma f_{10} + \nu' f_{01} + \sigma\nu' f_{11} + \ldots,$$
$$g = g_{00} + \sigma g_{10} + \nu' g_{01} + \sigma\nu' g_{11} + \ldots,$$

where we have dropped the superscript tilde since for the rest of the theoretical calculations we shall be working exclusively with the scaled terms.

The leading terms of (10) and (11) are now $(\partial^2/\partial t^2 + 1)f_{00} = 0$ and $\partial^2 g_{00}/\partial t^2 = 0$. Rejecting the possibility that g_{00} grows linearly in the fastest time variable (since g is proportional to the amplitude of the low frequency mode) we have

$$\left.\begin{aligned} f_{00} &= a\cos(t + \Delta\tau) + b\sin(t + \Delta\tau), \\ g_{00} &= g_{00}(\tau, T), \end{aligned}\right\} \tag{12}$$

where a and b are independent of t.

The next pair of equations presenting any new structure is

$$\left.\begin{aligned}\left(\frac{\partial^2}{\partial t^2}+1\right)f_{10} &= -2\frac{\partial^2}{\partial t\,\partial\tau}f_{00}-2\nu\frac{\partial}{\partial t}f_{00}-2\alpha f_{00}g_{00}-2\lambda f_{00}^3+4B\cos(t+\Delta\tau),\\ \partial^2 g_{20}/\partial t^2 &= -(\partial^2/\partial\tau^2+1)\,g_{00}.\end{aligned}\right\} \tag{13}$$

We reject the possibility that g_{20} grows quadratically (or even linearly) on the fastest time scale, and it follows that

$$g_{00} = c(T)\cos(\tau+\theta(T)). \tag{14}$$

The solution for f_{10} grows linearly on the time scale t unless the inhomogeneous terms in (13) satisfy the non-secularity conditions

$$\left.\begin{aligned}\partial a/\partial\tau+\nu a+\Delta b-\alpha b g_{00}-\tfrac{3}{4}\lambda b(a^2+b^2) &= 0,\\ \partial b/\partial\tau+\nu b-\Delta a+\alpha a g_{00}+\tfrac{3}{4}\lambda a(a^2+b^2) &= 2B.\end{aligned}\right\} \tag{15}$$

It can be shown that when $\lambda B^2/\nu^3$ is not large the solution of these equations tends exponentially fast (at the rate $e^{-\nu\tau}$) to a solution with period 2π. For the experiment described in § 6, this merely tells us that when the system is turned on the transients disappear on a time scale of 1 s.

Finally, we need to consider the $\tilde{\nu}'$ coefficient in (11):

$$\frac{\partial^2}{\partial t^2}g_{12} = -\left(\frac{\partial^2}{\partial\tau^2}+1\right)g_{01}-2\frac{\partial^2}{\partial\tau\,\partial T}g_{00}-2\frac{\partial}{\partial\tau}g_{00}-\beta f_{00}^2-2\kappa g_{00}^3.$$

The condition that g_{12} cannot grow quadratically on the fastest time scale implies that g_{01} must satisfy

$$\left(\frac{\partial^2}{\partial\tau^2}+1\right)g_{01} = -2\frac{\partial^2}{\partial\tau\,\partial T}g_{00}-2\frac{\partial}{\partial\tau}g_{00}-\tfrac{1}{2}\beta(a^2+b^2)-2\kappa g_{00}^3,$$

and the condition that g_{01} cannot grow linearly on the middle time scale is that

$$\left.\begin{aligned}\partial c/\partial T+c-\tfrac{1}{4}\beta\{\sin(\tau+\theta)\text{ coefficient of }(a^2+b^2)\} &= 0,\\ \partial\theta/\partial T+(\beta/4c)\{\cos(\tau+\theta)\text{ coefficient of }(a^2+b^2)\}-\tfrac{3}{4}\kappa c^2 &= 0,\end{aligned}\right\} \tag{16}$$

where for algebraic convenience we have assumed that a and b are the strictly periodic solutions of (15).

4. Onset of instability

When the low frequency wave amplitude $c(T)$ is negligible, we can solve (15) to obtain the familiar response curve for a soft spring:

$$2B = A[\nu^2+(\tfrac{3}{4}\lambda A^2-\Delta)^2]^{\frac{1}{2}}, \tag{17}$$

where A denotes the steady value of $(a^2+b^2)^{\frac{1}{2}}$.

During the onset of any instability, the periodic solution of (15) can be represented as a perturbation about the steady solution:

$$a+ib = \frac{A(1+cz)\,(\nu+i[\Delta-\tfrac{3}{4}\lambda A^2])}{|\nu+i(\Delta-\tfrac{3}{4}\lambda A^2)|},$$

and to first order in c we find that z satisfies the equation

$$dz/d\tau + \nu z - i\Delta z + \tfrac{3}{4}\lambda i A^2(2z + z^*) = -i\alpha\cos(\tau + \theta).$$

After a straightforward but lengthy calculation, we find that the $\sin(\tau+\theta)$ coefficient of the periodic solution for z has real part

$$\frac{2\nu\alpha(\Delta - \frac{3}{4}\lambda A^2)}{4\nu^2 + \{(\Delta - \frac{3}{4}\lambda A^2)(\Delta - \frac{9}{4}\lambda A^2) + \nu^2 - 1\}^2}.$$

To first order in c, the $\sin(\tau+\theta)$ coefficient of a^2+b^2 is simply equal to $2A^2c$ times this expression, and so (16) becomes

$$\frac{dc}{dT} + c\left\{1 - \frac{A^2\nu\alpha\beta(\Delta - \frac{3}{4}\lambda A^2)}{4\nu^2 + \{(\Delta - \frac{3}{4}\lambda A^2)(\Delta - \frac{9}{4}\lambda A^2) + \nu^2 - 1\}^2}\right\} = 0.$$

Thus the amplitude of the low frequency wave either grows or decays exponentially fast depending on whether the sound intensity A^2 exceeds or is less than the critical value A_c^2 which satisfies the implicit equation

$$A_c^2 = \frac{4\nu^2 + \{(\Delta - \frac{3}{4}\lambda A_c^2)(\Delta - \frac{9}{4}\lambda A_c^2) + \nu^2 - 1\}^2}{\nu\alpha\beta(\Delta - \frac{3}{4}\lambda A_c^2)}. \tag{18}$$

We note that the presence of the λ terms means that the neutral-stability curve has an asymptote at the nonlinear resonance frequency $\Delta = \frac{3}{4}\lambda A_c^2$.

5. Hysteresis

We define a function S via

$$cS = \tfrac{1}{4}\beta\{\sin(\tau+\theta) \text{ coefficient of } (a^2+b^2)\}, \tag{19}$$

where a and b are the periodic solutions of (15). In terms of S we can now rewrite (16) as

$$dc/dT + c(1-S) = 0.$$

The condition for onset of instability is that $S > 1$ at $c = 0$, and the wave amplitude will continue to grow until S is reduced to the value unity. If the driving frequency $\Omega + \Delta\sigma$ or the driving amplitude B is then gradually changed, c will adjust so that $S = 1$ again. During this adjustment, the perturbation $\mathscr{C}$ of the low frequency wave amplitude away from its steady value satisfies

$$d\mathscr{C}/dT - \mathscr{C}\,\partial S/\partial c = O(\mathscr{C}^2)$$

and decays exponentially fast provided that $\partial S/\partial c < 0$. If, however, this is violated at some stage, there will be a rapid increase in the value of c until the next root of $S = 1$.

It is noteworthy that the abrupt transitions necessarily increase the value of c. Thus, at one particular setting of drive and frequency, there could be more than one stable solution for c; the lower branch would be obtained if the drive was suddenly switched on (so that c was initially infinitesimal), and the higher branch would be obtained either by slowly reducing the drive from some large value or

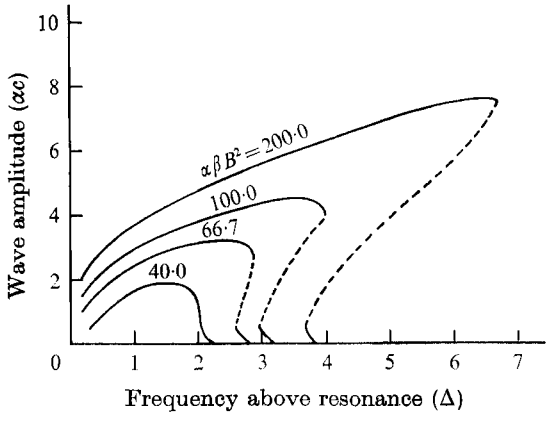

FIGURE 3. Theoretical hysteresis curves. ——, stable steady solutions at constant drive; – – – –, unstable steady solutions at constant drive.

else by changing the frequency from a value at which there was only one stable solution for c.

Hysteresis has only been observed experimentally at frequencies well above resonance and at sound intensities such that the nonlinear frequency shift terms in (15) are dominated by the Δ terms. Thus it is natural to assume that the cubic nonlinearities do not play a vital role in hysteresis, and for algebraic simplicity we shall ignore them. The solution to (15) is then

$$a+ib = \exp[-\nu\tau + i(\Delta\tau - \alpha c \sin\tau)] \times \left\{(a+ib)|_{\tau=0} + 2iB\int_0^\tau \exp[\nu t - i(\Delta t - \alpha c \sin t)]\,dt\right\},$$

where the constant of integration is chosen to ensure a periodic solution, and without loss of generality we have ignored the phase shift θ. A second integration is required to determine the function S (which in the absence of the cubic nonlinearities is proportional to αB^2).

Figure 3 shows the relationship between the dimensionless quantities αc, Δ and $\alpha\beta B^2$ which holds when $\tilde{\nu}$ has the value relevant to the experiments described in § 6; these curves were determined numerically by Mr T. Sprinks at the University of Essex. (For large values of Δ and αc we can derive asymptotic expansions for a and b and hence for $\alpha\beta B^2$. These analytical expressions, however, are extremely complicated and merely provide a check on the accuracy of the numerical quadratures.) For $\Delta > 3$ it can be seen that the constant-drive response curves have the overturning that is characteristic of hysteresis.

6. Experimental investigation

A deep rectangular tank was constructed and was filled with water to within 3·81 cm of the lid, the air space so formed resembling an organ pipe. When this resonance chamber was excited near an acoustic resonance frequency, a standing surface water wave could be generated. This water wave was of very much lower

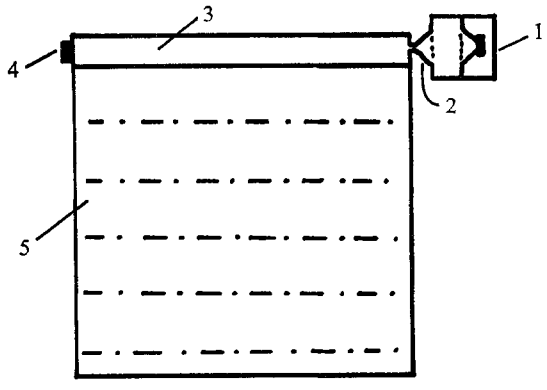

FIGURE 4. Diagram of experimental apparatus. (1) Loudspeaker driving unit, (2) conical coupler, (3) resonance chamber, (4) microphone, (5) water.

frequency than the acoustic wave (typically by a ratio 1:200), and had a wavelength half that of the acoustic wave.

We here aim to check two predictions of the previous theory: the expression (18) for the neutral-stability curves, and the general shape of the water-wave response curves given in figure 3. In order to determine the parameters λ and ν, we shall also make use of (17).

6.1. *Apparatus*

The apparatus, which is shown diagrammatically in figure 4, was a rectangular tank (constructed from $\frac{3}{8}$ in. Perspex sheets) with internal dimensions: length, 60·5 cm; depth, 60·5 cm; breadth, 10·0 cm. All joints were glued except those at the top, the lid being sealed with a silicone rubber preparation and then screwed down. The 6 in. loudspeaker was mounted on a central baffle in a padded box and connected to the 3·81 cm deep resonance chamber by a conical polythene funnel passing through a $\frac{3}{4}$ in. hole drilled in the end face of the tank. At the opposite end of the chamber a 1 in. crystal microphone insert was flush mounted into the end wall. The loudspeaker was driven by the amplified signal from a stabilized oscillator, and an electronic counter was used to record the working frequency correct to within 0·05 Hz. The acoustic field was detected by the crystal microphone in the end wall and the resulting signal displayed on an oscilloscope. This microphone was later calibrated against a 1 in. condenser microphone using a Brüel & Kjaer Precision Sound Level Meter Type 2203. The water-wave amplitude was measured using a capacitance probe mounted on the lid of the tank, the resulting signal being displayed on the (double-beam) oscilloscope. This was later calibrated statically by noting the output voltage from the probe as the water level was changed. Thus although the probe was being used outside its linear range, a calibration was available for all wave heights encountered.

6.2. *Measurement of basic parameters*

The acoustic resonance frequencies were determined by noting the frequencies at which the microphone output rose to a maximum as the driving frequency was varied at constant (low) power input. Initial experiments showed that the system

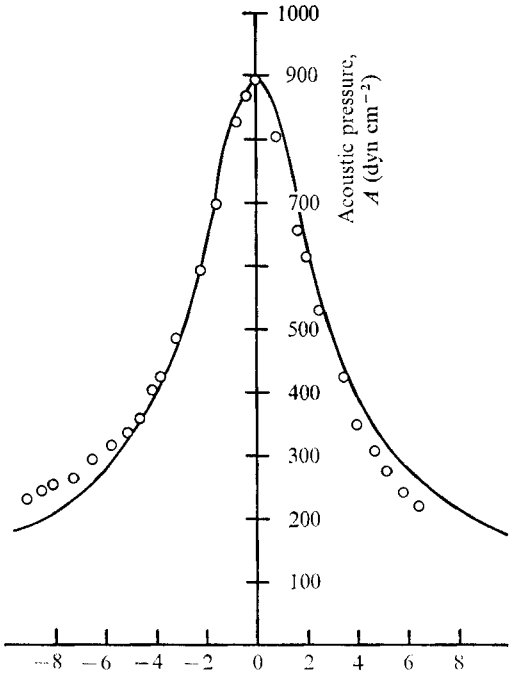

FIGURE 5. Theoretical and experimental response curves. ——, theory; ○, experiment.

Parameter	Value
$2\pi/\sigma$ (s)	0·613
$\sigma\tilde{\nu}'$ (s^{-1})	0·043
ν (s^{-1})	20·20
Ω (s^{-1})	1880

TABLE 2. Experimental values of the parameters $2\pi/\sigma$, $\sigma\tilde{\nu}'$, ν and Ω

was highly sensitive to temperature changes, and so throughout the experiments the appropriate resonance was determined for each run and the results compared through the use of the parameter Δ.

Mahony & Smith proposed that the value of ν, the logarithmic decay rate for the acoustic mode, should be supplied from experiments. This was done by plotting the frequency response curve and fitting it to (17). Thus the variation in the acoustic response was measured as a function of frequency (for constant low input power), and (17) was then fitted to the results by matching the maximum value of A^2 and performing a least-squares calculation to yield ν. The agreement between these two curves is shown in figure 5.

The resonance frequency and decay rate of the water wave were measured in two ways. The wave was either excited acoustically (that is, by the mechanism of spatial resonance) or manually (using a plunger), and its period $2\pi/\sigma$ and decay rate $\sigma\tilde{\nu}'$ were measured over a large number of cycles using a stop-watch. These figures, together with the value of ν and Ω, are given in table 2.

6.3. *Neutral-stability curve*

In the present experiments the growth rates were sufficiently small to enable a direct measurement of A_c to be made. Thus, having selected a working frequency, the driving amplitude B was slowly increased until a water wave was just discernable from the oscilloscope trace. The value of A corresponding to this value of B was then noted as A_c for the frequency under consideration. This process was then repeated for all the required frequencies and hence the neutral-stability curve was built up.

6.4. *Hysteresis curves*

Hysteresis in the water-wave amplitude can be observed in two ways: either by keeping the drive constant and slowly varying the frequency, or by keeping the frequency constant and slowly varying the drive. For ease of comparison with the previous theory, we consider here only the former method.

For each run, the input power was held constant at a certain value and Δ was increased in steps by adjusting the driving frequency. After a pause to ensure that there was a steady state, the surface displacement was noted from the capacitance probe oscilloscope trace. Eventually a value of Δ was reached at which the surface-wave amplitude fell to zero. Starting from this value, readings were now taken as Δ was decreased to a lower limit at which the surface-wave amplitude was again zero.

7. Comparison of experimental and theoretical results

To plot the theoretical neutral-stability curve we require the experimental value of the constant λ. This would normally be obtained from (17) (after plotting a frequency response curve), but unfortunately the large surface wave made it impossible to determine A with any accuracy. Thus a least-squares fit was performed on the experimental neutral-stability data, and the value $\tilde{\lambda} = -1{\cdot}58 \times 10^{-8}$ obtained from this. This is consistent with a tentative evaluation as described above. The theoretical and experimental neutral-stability curves are given in figure 6.

Figure 7 shows the experimental hysteresis curves for several values of the drive B, the value of α being obtained from Mahony & Smith's equations (13) and (14). [We note here an error in the paper by Mahony & Smith: the value of β is given incorrectly and should be, using their notation,

$$\beta = \frac{1}{2\sigma}\left(\frac{\rho_a}{\rho}\right)\left(\frac{m\pi}{l}\right)\left\{\left(\frac{m\pi}{l}\right)^2 + \left(\frac{\omega}{c}\right)^2\right\}.$$

This, of course, slightly alters the theoretical values of $\alpha\beta$ quoted by Franklin, Price & Williams.]

The agreement between theory and experiment is thought to be quite satisfactory, answering in main part the questions raised by Franklin, Price & Williams.

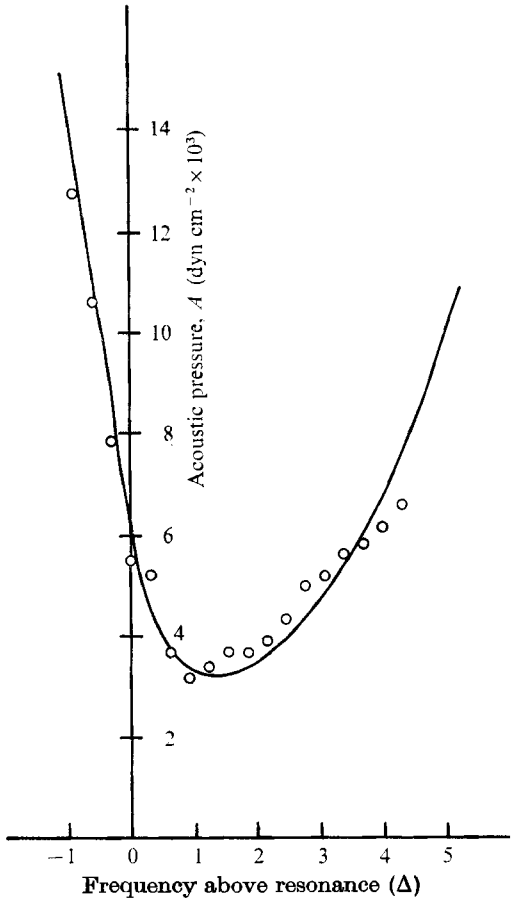

FIGURE 6. Theoretical and experimental neutral-stability curves. ——, theory; ○, experiment.

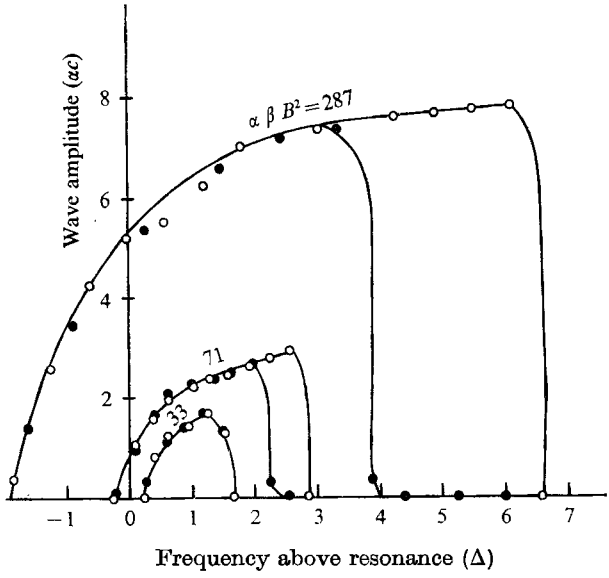

FIGURE 7. Experimental hysteresis curves. ○, increasing frequency; ●, decreasing frequency.

The authors would like to record their gratitude to Mr T. Sprinks of the Mathematics Department at the University of Essex for the computational work contained in this paper and to the referees for many helpful comments. One of us (I.D.H.) gratefully acknowledges the receipt of an S.R.C. Studentship.

REFERENCES

COLE, J. D. 1968 *Perturbation Methods in Applied Mathematics.* Waltham, Mass.: Blaisdell.

FRANKLIN, R. E., PRICE, M. & WILLIAMS, D. C. 1973 Acoustically driven water waves. *J. Fluid Mech.* **57**, 257–268.

HUNTLEY, I. 1972 Observations on a spatial-resonance phenomenon. *J. Fluid Mech.* **53**, 209–216.

MAHONY, J. J. & SMITH, R. 1972 On a model representation for certain spatial-resonance phenomena. *J. Fluid Mech.* **53**, 193–208.